

STUDY OF A LOW MACH NUCLEAR CORE MODEL FOR SINGLE-PHASE FLOWS

MANUEL BERNARD¹, STÉPHANE DELLACHERIE², GLORIA FACCANONI³, BÉRÉNICE GREC⁴, OLIVIER LAFITTE⁵, TAN-TRUNG NGUYEN⁶ AND YOHAN PENEL¹

Abstract. This paper deals with the modelling of the coolant (water) in a nuclear reactor core. This study is based on a monophasic low Mach number model (LMNC model) coupled to the stiffened gas law for a single-phase flow. Some analytical steady and unsteady solutions are presented for the 1D case. We then introduce a numerical scheme to simulate the 1D model in order to assess its relevance. Finally, we carry out a normal mode perturbation analysis in order to approximate 2D solutions around the 1D steady solutions.

Résumé. Dans cet article, nous nous intéressons à la modélisation de l'écoulement de l'eau dans le circuit primaire d'un réacteur nucléaire. Pour cela, nous utilisons un modèle bas-Mach monophasique (modèle LMNC) pour une loi d'état de type gaz raidi. Nous présentons des solutions analytiques 1D stationnaires et instationnaires pour certains types de données. Nous simulons ensuite le modèle afin d'évaluer sa pertinence. La dernière partie est consacrée à une analyse de perturbations en modes normaux réalisée pour approcher les solutions 2D à partir des solutions stationnaires 1D.

INTRODUCTION

In the framework of safety evaluations in nuclear reactor cores, several models have been derived [4, 5] in order to better understand the evolution of physical variables (like temperature) within the reactor. Let us first present the normal functioning of a PWR (Pressurized Water Reactor) – see FIG. 1.

In a PWR, the primary coolant (water) is pumped under high pressure to the reactor core where it is heated (by the energy generated by the fission of atoms) by thermal conduction through the fuel cladding. Pressure in the primary coolant loop (approximately $155 \cdot 10^5$ Pa) prevents water from boiling within the reactor. The heated water then flows to a steam generator where it transfers its thermal energy to a secondary system

¹ INRIA Lille - Nord Europe, Parc Scientifique de la Haute Borne, 40 avenue Halley, 59658 Villeneuve d'Ascq, France
& e-mail: manuel.bernard@ifpen.fr & e-mail: yohan.penel@gmail.com

² DEN/DANS/DM2S/STMF, Commissariat à l'Énergie Atomique Saclay, 91191 Gif-sur-Yvette, France
& e-mail: stephane.dellacherie@cea.fr

³ IMATH - Université du Sud Toulon-Var, avenue de l'Université, 83957 La Garde, France
& e-mail: faccanoni@univ-tln.fr

⁴ MAP5 UMR CNRS 8145 - Université Paris Descartes - Sorbonne Paris Cité, 45 rue des Saints Pères, 75270 Paris Cedex 6, France & e-mail: berenice.grec@parisdescartes.fr

⁵ LAGA UMR 7539 - Institut Galilée - Université Paris 13, 99 avenue Jean-Baptiste Clément, 93430 Villetaneuse, France
& e-mail: lafitte@math.univ-paris13.fr

⁶ LATP UMR 6632 - Université de Provence, Technopôle Château-Gombert, 39 rue F. Joliot Curie, 13453 Marseille Cedex 13, France

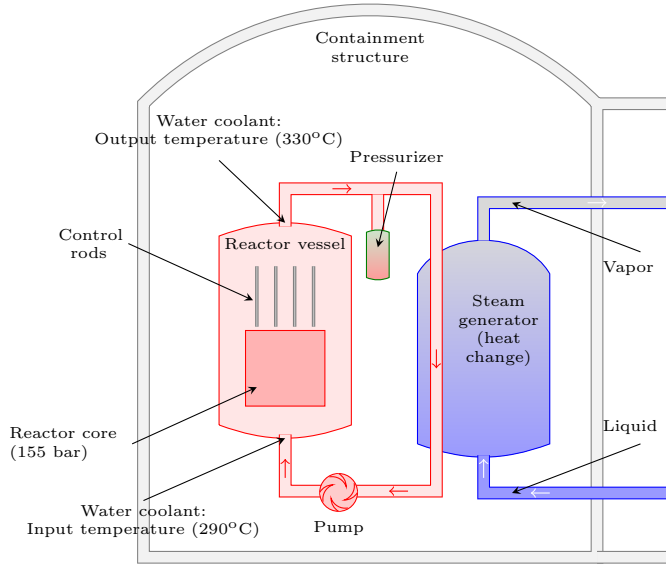


FIGURE 1. Scheme of the primary circuit of a PWR.

where steam is generated and flows to a turbine which, in turn, spins an electric generator. The transfer of heat is accomplished without mixing the two fluids, which is desirable since the primary coolant might become radioactive.

Due to the order of magnitude of the physical quantities, the flow in the core of a PWR can be considered as a low Mach number flow when the situation is nominal or in some accidental situations. In [4], the author formally derives a low Mach number model (called LMNC for *Low Mach Nuclear Core model*) describing the evolution of the coolant (in liquid phase) inside a nuclear reactor core. This system of PDEs includes a source term (power density) modelling the heating due to fission reactions as well as inlet and outlet boundary conditions.

The outline of this paper is the following. In section 1, we recall the model for a 1D single-phase flow together with the stiffened gas law and we present analytical steady and unsteady solutions. Section 2 is devoted to numerical simulations of the model by means of a numerical method of characteristics. In section 3, we perform a normal mode perturbation analysis around the 1D steady solution in order to provide an approximation of 2D solutions.

1. A 1D SINGLE-PHASE LOW-MACH MODEL

The LMNC model is an initial boundary value problem derived in [4]. As the Mach number of the flow is assumed to be very small, an asymptotic expansion (wrt to the Mach number) can be performed in the compressible Navier-Stokes equations similarly to [10]. The LMNC model then corresponds to order 0 in this expansion. The main consequences of this low Mach number approach are the fact that a single time scale can be taken into account and the decoupling between the thermodynamic pressure p_0 (which is a constant in this study) and the dynamic pressure \bar{p} .

1.1. Governing equations

We consider in this section the one-dimensional case where the direction corresponds to the “vertical” axis relatively to FIG. 1. The origin $y = 0$ corresponds to the bottom of the core and $y = L$ to the top. The model

reads:

$$\begin{cases} \partial_t \rho + \partial_y(\rho v) = 0, & (1a) \\ \partial_t(\rho h) + \partial_y(\rho h v) = \Phi, & (1b) \\ \partial_t(\rho v) + \partial_y(\rho v^2 + \bar{p}) - \mu_0 \partial_{yy}^2 v = -\rho g, & (1c) \end{cases}$$

in the bounded domain $\Omega = (0, L)$. Phase transition is not taken into account in the present study, which means that the fluid is supposed to remain monophasic. Here, ρ denotes the density of the fluid, v its velocity, h its enthalpy, μ_0 the constant viscosity¹ and g the gravity. The nuclear fission reaction is modelled by the source term $\Phi = \Phi(t, y)$ called the power density. We assume in the sequel that $\Phi(t, y) \geq 0$ for all $t \geq 0$ and $y \in \Omega$.

To close the system, an additional equation is required, namely an equation of state (EOS) connecting thermodynamic variables. This relation is assumed to guarantee the positivity of relevant quantities such as density or pressure. In the present study, we consider an EOS of the form:

$$\rho = \rho(h, p_0). \quad (2)$$

We also impose initial and boundary conditions:

$$h(0, y) = h_0(y), \quad (\rho v)(0, y) = D_0(y), \quad (3)$$

$$h(t, 0) = h_e(t), \quad (\rho v)(t, 0) = D_e(t), \quad \bar{p}(t, L) = p_0, \quad (4)$$

for given functions $h_0(y)$, $D_0(y) \geq 0$, $h_e(t)$ and $D_e(t) \geq 0$. The positivity hypotheses correspond to an upward flow which is natural in this context. Conditions (4) mean that the fluid is injected at the bottom of the core at a given enthalpy and at a given flow rate and that the outlet pressure is imposed.

It is worth underlining that $\rho(0, \cdot)$ and $\rho(\cdot, 0)$ are deduced from EOS (2) with h_0 and h_e respectively. Velocities $v(0, \cdot)$ and $v(\cdot, 0)$ are then computed as $D_0/\rho(0, \cdot)$ and $D_e/\rho(\cdot, 0)$. The dependence of inlet data with respect to time enables to model transient regimes induced by accidental situations. For example, the decrease of $D_e(t)$ towards 0 as t increases models a main coolant pump trip event which is a Loss Of Flow Accident (LOFA) as at the beginning of the Fukushima accident in reactors 1, 2 and 3.

As detailed in [1, 4], this system may be expressed differently in order to highlight that one of the variables (ρ, h, v, \bar{p}) might be considered as a parameter through the equation of state: hence one has to choose to select one variable in (ρ, h) . We decided to keep (h, v, \bar{p}) as main variables. This leads to the new (non-conservative) formulation:

$$\begin{cases} \partial_y v = \frac{\beta(h, p_0)}{p_0} \Phi, & (5a) \end{cases}$$

$$\begin{cases} \partial_t h + v \partial_y h = \frac{\Phi}{\rho(h, p_0)}, & (5b) \end{cases}$$

$$\begin{cases} \rho(h, p_0) (\partial_t v + v \partial_y v) - \mu_0 \partial_{yy}^2 v = -\partial_y \bar{p} - \rho(h, p_0) g. & (5c) \end{cases}$$

The equivalence between (1) and (5) relies on smoothness assumptions [1]. Eq. (5a) is a reformulation of (1a) and shows that the model is still compressible ($\partial_y v \neq 0$) despite a small Mach number. The (nondimensional) compressibility coefficient β is defined by:

$$\beta(h, p_0) \stackrel{\text{def}}{=} -\frac{p_0}{\rho^2} \frac{\partial \rho}{\partial h}.$$

¹The viscosity is assumed to be constant for the sake of simplicity and without loss of generality. For the general case, we can impose a constitutive law $\mu(h, p_0)$.

Phase	c_v [J · K ⁻¹]	γ	π [Pa]	q [J · kg ⁻¹]
Liquid	1816.2	2.35	10 ⁹	-1167.056 × 10 ³
Vapor	1040.14	1.43	0	2030.255 × 10 ³

TABLE 1. Water and steam, parameters computed in [7, 8].

1.2. Equation of state

The equation of state that will be used in the sequel is the stiffened gas law. It is a generalization of the well-known ideal gas law which is relevant for the liquid phase (for more details see for example [7, 8]). In the present case, this EOS can be written:

$$\rho(h, p) = \frac{\gamma}{\gamma - 1} \frac{p + \pi}{h - q} \quad \text{for } h > q, \tag{6}$$

where the parameters $\gamma > 1$ (adiabatic coefficient), π (molecular attraction) and q (binding energy) are constants describing thermodynamic properties of the fluid. Examples are given in TAB. 1. Notice that for $\pi = 0$ and $q = 0$, we recover the ideal gas law. For the sake of simplicity, since p_0 is constant, we denote $\rho(h) \stackrel{\text{def}}{=} \rho(h, p = p_0)$.

An important consequence of this choice of equation of state is that the compressibility coefficient β is constant and equal to:

$$\beta_0 \stackrel{\text{def}}{=} \beta(h, p = p_0) = \frac{\gamma - 1}{\gamma} \frac{p_0}{p_0 + \pi}.$$

We can also express other thermodynamic variables as functions of h such as the temperature T and the speed of sound c^* . More precisely, T is defined by the relation:

$$T(h) = \frac{h - q}{\gamma c_v},$$

where the constant c_v is the specific heat at constant volume. Likewise, denoting by s the entropy of the fluid, we have:

$$c^*(h) \stackrel{\text{def}}{=} \left(\sqrt{\left(\frac{\partial p}{\partial \rho} \right)_{|s=\text{cst}}} \right) (h, p = p_0) = \sqrt{(\gamma - 1)(h - q)}.$$

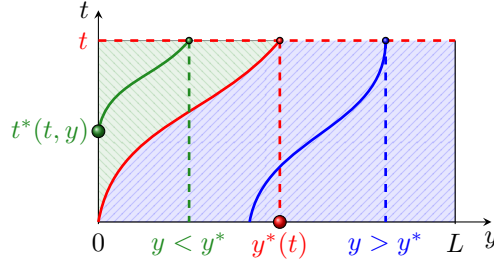
1.3. Analytical solutions

We consider Syst. (5) together with conditions (3-4) and EOS (6). Steady solutions have been computed in [4, Lemma 4.1] and provide reliable elements to compare with numerical solutions. However, it is also possible to derive explicit unsteady solutions in numerous cases depending on Φ , in particular when Φ is constant or a function of y only. The proof of the present results will be detailed in [1]. The following analysis is based on the method of characteristics. Indeed, as β_0 does not depend on h anymore, Eq. (5a) is decoupled from (5b-5c) and can be integrated directly:

$$v(t, y) = v_e(t) + \frac{\beta_0}{p_0} \Psi(t, y), \quad \Psi(t, y) \stackrel{\text{def}}{=} \int_0^y \Phi(t, z) \, dz. \tag{7}$$

The method of characteristics is then applied to solve Eq. (5b) which can be rewritten given EOS (6) as:

$$\partial_t h + v \partial_y h = \frac{\beta_0 \Phi}{p_0} (h - q).$$

FIGURE 2. Sketch of the method of characteristics and definitions of y^* and t^* .

1.3.1. Constant power density and constant inlet velocity

The first case we handle in this paper is the constant Φ case: $\Phi(t, y) \equiv \Phi_0$. We also assume that $v_e(t) \equiv v_e > 0$. We set $\hat{\Phi}_0 \stackrel{\text{def}}{=} \beta_0 \Phi_0 / p_0$. Then $v(t, y) = v(y) = v_e + \hat{\Phi}_0 y$ and:

$$h(t, y) = \begin{cases} q + \left[h_0 \left(\left\{ y + \frac{v_e}{\hat{\Phi}_0} \right\} e^{-\hat{\Phi}_0 t} - \frac{v_e}{\hat{\Phi}_0} \right) - q \right] e^{\hat{\Phi}_0 t}, & \text{if } y \geq y^*(t), \\ q + (h_e(t^*) - q) \left(1 + \frac{\hat{\Phi}_0}{v_e} y \right), & \text{if } y < y^*(t), \end{cases} \quad (8)$$

where $y^*(t) \stackrel{\text{def}}{=} v_e \frac{e^{\hat{\Phi}_0 t} - 1}{\hat{\Phi}_0}$ and for $y < y^*(t)$, $t^*(t, y) \stackrel{\text{def}}{=} t - \frac{1}{\hat{\Phi}_0} \ln \left(1 + \frac{\hat{\Phi}_0}{v_e} y \right)$. See FIG. 2 for notations.

We then compute \bar{p} by integrating Eq. (5c) and remarking that $\partial_{yy}^2 v = 0$. For $y \geq y^*(t)$, we have:

$$\bar{p}(t, y) = p_0 \left\{ 1 + \left(\frac{g + \hat{\Phi}_0 v_e e^{\hat{\Phi}_0 t}}{\beta_0} \right) \left[H_0 \left(\left\{ L + \frac{v_e}{\hat{\Phi}_0} \right\} e^{-\hat{\Phi}_0 t} - \frac{v_e}{\hat{\Phi}_0} \right) - H_0 \left(\left\{ y + \frac{v_e}{\hat{\Phi}_0} \right\} e^{-\hat{\Phi}_0 t} - \frac{v_e}{\hat{\Phi}_0} \right) \right] \right. \\ \left. + \frac{\hat{\Phi}_0^2}{\beta_0} e^{\hat{\Phi}_0 t} \left[\mathcal{H}_0 \left(\left\{ L + \frac{v_e}{\hat{\Phi}_0} \right\} e^{-\hat{\Phi}_0 t} - \frac{v_e}{\hat{\Phi}_0} \right) - \mathcal{H}_0 \left(\left\{ y + \frac{v_e}{\hat{\Phi}_0} \right\} e^{-\hat{\Phi}_0 t} - \frac{v_e}{\hat{\Phi}_0} \right) \right] \right\}, \quad (9a)$$

where H_0 and \mathcal{H}_0 are some primitive functions of $z \mapsto [h_0(z) - q]^{-1}$ and of $z \mapsto z[h_0(z) - q]^{-1}$. For $y < y^*(t)$, we have:

$$\bar{p}(t, y) = \bar{p}(t, y^*(t)) + \frac{p_0 v_e}{\beta_0} \left\{ g \left[H_e \left(t - \frac{1}{\hat{\Phi}_0} \ln \left(1 + \frac{\hat{\Phi}_0}{v_e} y \right) \right) - H_e(0) \right] \right. \\ \left. + \hat{\Phi}_0 v_e \left[\mathcal{H}_e \left(t - \frac{1}{\hat{\Phi}_0} \ln \left(1 + \frac{\hat{\Phi}_0}{v_e} y \right) \right) - \mathcal{H}_e(0) \right] \right\}, \quad (9b)$$

where $\bar{p}(t, y^*(t))$ is computed by taking $y = y^*(t)$ in (9a) and H_e, \mathcal{H}_e are some primitive functions of $z \mapsto [h_e(z) - q]^{-1}$ and of $z \mapsto z[h_e(z) - q]^{-1}$. For the proof of (8) and (9), the reader may refer to [1].

Let us make a few comments about these results. First of all, we recover steady solutions from [4] when h_e is constant. Indeed y^* is an unbounded monotone-increasing function of t which implies that, for a given $y \in (0, L)$, we can find t large enough such that $y^*(t) > y$. Moreover, defining $t_\infty \stackrel{\text{def}}{=} \frac{1}{\hat{\Phi}_0} \ln \left(1 + \frac{\hat{\Phi}_0 L}{v_e} \right)$ (*i.e.* such that $y^*(t_\infty) = L$), we have:

$$\forall t \geq t_\infty, h(t, y) = q + (h_e - q) \left(1 + \frac{\hat{\Phi}_0}{v_e} y \right) = h_e + \frac{\hat{\Phi}_0}{D_e} y \stackrel{\text{def}}{=} h_\infty(y).$$

The asymptotic state is thus reached in finite time. It can also be inferred from (8) that at a fixed time $t < t_\infty$, $h(t, y) = h_\infty(y)$ for all $y \leq y^*(t)$. The same conclusions hold when h_e is a bounded function which reaches its upper bound in finite time. For unbounded h_e , as $t^*(t, y) \xrightarrow{t \rightarrow +\infty} +\infty$, then $h(t, y) \xrightarrow{t \rightarrow +\infty} +\infty$ which can be easily accounted for: *if the inlet enthalpy indefinitely increases, the system cannot allow for steady states.*

Remark 1.1. The case of a non-constant inlet velocity also provides a solution but which is no more explicit: $y^*(t)$ then depends on the primitive function of $\tau \mapsto v_e(\tau)e^{-\hat{\Phi}_0\tau}$. As for the case of a vanishing inlet velocity, the same calculations can be carried out and show that $h(t, y) \xrightarrow{t \rightarrow +\infty} +\infty$ no matter what h_e is: *if the pumps stop, the fluid is constantly heated and the enthalpy increases.*

Remark 1.2 (comparison with experimental data). Expression (8) then enables to compare with experimental data (denoted by the exponent exp in the sequel) in a PWR with $L = 4.2$ m. In a nominal situation, the steady state is characterized by $p_0 = 155 \cdot 10^5$ Pa, $\rho_e^{\text{exp}} \approx 750$ kg · m⁻³ and $v_e^{\text{exp}} \approx 5$ m · s⁻¹. Measurements yield $\rho^{\text{exp}}(L) \approx 650$ kg · m⁻³ and $T^{\text{exp}}(L) \approx 583$ K [13].

To assess the relevance of our model, we can consider as a first approximation that the power density is constant and equal to 170 MW · m⁻³. Parameters of EOS (6) for the water (in liquid phase) are taken as in TAB. 1. Thus $h(t, 0) \approx 1.18 \cdot 10^6$ J · K⁻¹. No matter what the initial datum h_0 , the asymptotic state is reached at time $t_\infty \approx 0.81$ s and we obtain:

$$\rho(t, L) \approx 694 \text{ kg} \cdot \text{m}^{-3} \quad \text{and} \quad T(t, L) \approx 597 \text{ K} \quad \text{for } t \geq t_\infty.$$

These results are of the same order as experimental values. The discrepancy may be explained by the fact that some steam may appear at the top of the core which would require to introduce phase transition into the modelling. It will be handled in [1]. However, values in TAB. 1 may not be accurate for pressure p_0 (see [7]) and results may have to be improved, for instance with the use of tabulated laws [2].

1.3.2. Power density varying with y

Similar results can be proved for $\Phi(t, y) = \Phi(y)$ when $v_e(t) \equiv v_e > 0$ but this requires an additional notation: let Θ be the primitive function vanishing at 0 of $z \mapsto 1/v(z)$ with v given by (7). Note that Ψ also depends only on y and that Θ is a one-to-one monotone-increasing mapping. Then we have:

$$h(t, y) = \begin{cases} q + v(y) \frac{h_0(\Theta^{-1}(\Theta(y) - t)) - q}{v(\Theta^{-1}(\Theta(y) - t))}, & \text{if } y \geq y^*(t), \\ q + v(y) \frac{h_e(t^*) - q}{v_e}, & \text{if } y < y^*(t), \end{cases} \quad (10)$$

where $y^*(t) \stackrel{\text{def}}{=} \Theta^{-1}(t)$ and $t^*(t, y) \stackrel{\text{def}}{=} t - \Theta(y)$ (see FIG. 2). We still note $t_\infty \stackrel{\text{def}}{=} \Theta(L)$ for numerical applications.

For instance, when $\Phi \equiv \Phi_0$, then $\Theta(y) = \frac{1}{\hat{\Phi}_0} \ln \left(1 + \frac{\hat{\Phi}_0}{v_e} z \right)$ and we recover (8). When $\Phi(y) = (1 + y)\Phi_0$, then $\Theta(y) = \mathcal{A}(\arctan((1 + y)\mathcal{B}) - \arctan(\mathcal{B}))$, where $\mathcal{A} \stackrel{\text{def}}{=} 2p_0/\sqrt{\Phi_0\beta_0(2v_e p_0 - \beta_0\Phi_0)}$ and $\mathcal{B} \stackrel{\text{def}}{=} \mathcal{A}\beta_0\Phi_0/(2p_0)$.

Implicit expressions may also be given when $\Phi = \Phi(t)$ [1] but the general case $\Phi = \Phi(t, y)$ is still open.

2. SIMULATIONS OF THE 1D LMNC MODEL

Although explicit solutions to the problem (3-4-5-6) have been given in the previous section in some particular cases, it is relevant to design a numerical scheme in order to simulate the system in the general case. Expressions given in §§ 1.3.1 and 1.3.2 may help assess the performances of the numerical scheme which may then be used for arbitrary functions Φ . Notice that function Θ defined above may require a quadrature integration formula.

Given $\Delta y > 0$ and $\Delta t > 0$, we consider a uniform cartesian grid $\{y_i = i\Delta y\}_{1 \leq i \leq N}$ such that $y_1 = 0$ and $y_N = L$ (see FIG. 3) as well as a time discretization $\{t^n = n\Delta t\}_{n \geq 0}$. Unknowns are collocated at the nodes of the mesh. We set the initial values $v_i^0 = v_0(y_i)$ and $h_i^0 = h_0(y_i)$ for $i = 1, \dots, N$.

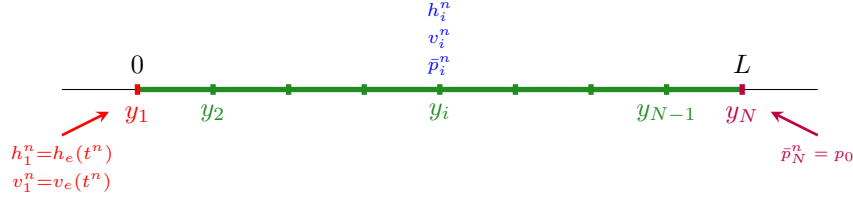


FIGURE 3. Grid and boundary conditions.

2.1. Numerical scheme

The key equation is (5b) due to the decoupling between equations in (5). As (5b) is a transport equation, a natural scheme is the numerical method of characteristics (MOC) [6,11]. This method is based on the equalities:

$$\frac{d}{dt} [h(t, \mathcal{Y}(t; t^{n+1}, y_i))] = \frac{\beta_0}{p_0} \Phi(t, \mathcal{Y}(t; t^{n+1}, y_i)) [h(t, \mathcal{Y}(t; t^{n+1}, y_i)) - q], \quad (11a)$$

where \mathcal{Y} is the solution to the ODE:

$$\begin{cases} \frac{d}{dt} \mathcal{Y}(t; t^{n+1}, y_i) = v(t, \mathcal{Y}(t; t^{n+1}, y_i)), & t \leq t^{n+1}, \\ \mathcal{Y}(t^{n+1}; t^{n+1}, y_i) = y_i. \end{cases} \quad (11b)$$

The overall process at time t^{n+1} consists of three steps (except for $i = 1$ where we impose $h_1^{n+1} = h_e(t^{n+1})$). Given the numerical solutions $(h_i^n, v_i^n, \bar{p}_i^n)$, the algorithm we shall apply in § 2.2 is:

- ① Solve ODE (11b) over the interval $[t^n, t^{n+1}]$. Let ξ_i^n be the numerical approximation of $\mathcal{Y}(t^n; t^{n+1}, y_i)$ – see [11]:
 - (i) $\xi_i^n = y_i - \Delta t \cdot v_i^n$ (order 1 in time);
 - (ii) $\xi_i^n = y_i - \Delta t \cdot v_i^n - \frac{1}{2} \Delta t^2 \left(\frac{v_i^n - v_i^{n-1}}{\Delta t} - \frac{\beta_0}{p_0} v_i^n \Phi(t^n, y_i) \right)$ (order 2 in time);
- ② Approximate the “upwind” enthalpy. The resolution of ODE (11a) involves the approximation \hat{h}_i^n of either $h(t^n, \xi_i^n)$ if $\xi_i^n \in (0, L)$ or $h_e(t^*)$ otherwise (see FIG. 4):
 - (i) If $\xi_i^n \geq 0$, set $t_i^* \stackrel{\text{def}}{=} t^n$; let j be the index such that $\xi_i^n \in [y_j, y_{j+1})$ and $\hat{h}_i^n = \theta_i^n h_j^n + (1 - \theta_i^n) h_{j+1}^n$ for $\theta_i^n = (y_{j+1} - \xi_i^n) / \Delta y$;
 - (ii) If $\xi_i^n < 0$, set $t_i^* \stackrel{\text{def}}{=} t^{n+1} - y_i / v_i^n$, $\xi_i^n = 0$ and $\hat{h}_i^n = h_e(t_i^*)$;
- ③ Update h_i^{n+1} by integrating ODE (11a) over $[t_i^*, t^{n+1}]$ (Euler scheme in time): $h_i^{n+1} = \hat{h}_i^n + (t^{n+1} - t_i^*) \frac{\beta_0}{p_0} \Phi(t_i^*, \xi_i^n) [\hat{h}_i^n - q]$.

The boundary $y = 0$ is the only one to care about since characteristic curves cannot exit from the core at $y = L$ (we assume that $v_e > 0$ and $\Phi \geq 0$ which implies that $v > 0$). The main feature of this scheme is that it is **unconditionally stable** (by construction). Furthermore, it preserves the positivity of temperature and density. Indeed, these variables have the same sign as $(h - q)$. Noticing that \hat{h}_i^n results from a convex combination and that:

$$h_i^{n+1} - q = \left(1 + (t^{n+1} - t_i^*) \frac{\beta_0}{p_0} \Phi(t_i^*, \xi_i^n) \right) (\hat{h}_i^n - q),$$

we conclude that if $h_i^n > q$ for all i , then $h_i^{n+1} > q$.

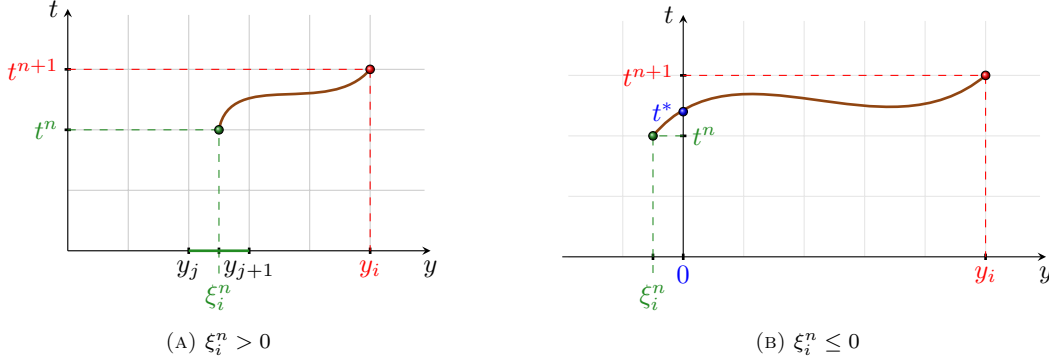


FIGURE 4. Numerical method of characteristics.

It remains to compute other variables:

- **Velocity.** Depending on the ability to compute the primitive function of Φ , the velocity field can be computed directly:

$$v_1^{n+1} = v_e(t^{n+1}),$$

$$v_i^{n+1} = v_{i-1}^{n+1} + \frac{\beta_0}{p_0} \int_{y_{i-1}}^{y_i} \Phi(t^{n+1}, z) dz, \quad i = 2, \dots, N,$$

or approximated by the following upwind approach (since $v_i^n \geq 0$ for all i and for all n):

$$v_i^{n+1} = v_{i-1}^{n+1} + \Delta y \frac{\beta_0}{p_0} \Phi(t^{n+1}, y_{i-1}).$$

- **Pressure.** \bar{p}^{n+1} is computed iteratively by rectangular formulae approximating the integral version of (5c) and using (5a):

$$\bar{p}_N^{n+1} = p_0,$$

$$\bar{p}_{i-1}^{n+1} = \bar{p}_i^{n+1} + \frac{\Delta y}{2} \left[(\rho(h_i^{n+1}) + \rho(h_{i-1}^{n+1}))g + \rho(h_i^{n+1}) \frac{v_i^{n+1} - v_i^n}{\Delta t} + \rho(h_{i-1}^{n+1}) \frac{v_{i-1}^{n+1} - v_{i-1}^n}{\Delta t} \right. \\ \left. + \rho(h_i^{n+1}) v_i^{n+1} \frac{\beta_0}{p_0} \Phi(t^{n+1}, y_i) + \rho(h_{i-1}^{n+1}) v_{i-1}^{n+1} \frac{\beta_0}{p_0} \Phi(t^{n+1}, y_{i-1}) \right] \\ - \mu_0 \frac{\beta_0}{p_0} [\Phi(t^{n+1}, y_i) - \Phi(t^{n+1}, y_{i-1})], \quad i \in \{2, \dots, N\}.$$

2.2. Numerical results

We apply in this section the numerical scheme presented in the previous paragraph to Syst. (5) for some particular functions Φ . All simulations have been carried out using MATLAB. The computational cost is about 1 minute for the finest grid. Figures for this section are positioned at the end of the paper.

Parameters are set as follows:

- (i) Geometry of the reactor: $L = 4.2$ m;
- (ii) Discretization parameters: $N = 50$ mesh nodes ($\Delta y \approx 0.086$), $\Delta t \approx 0.02$;

- (iii) Parameters involved in EOS (6): *cf.* TAB. 1 (liquid phase);
- (iv) Reference value for the pressure and the power density: $p_0 = 155 \cdot 10^5$ Pa, $\Phi_0 = 170$ MW \cdot m $^{-3}$;
- (v) Boundary data: $h_e = 1.236508 \cdot 10^6$ J \cdot kg $^{-1}$ (equivalent to $\rho_e = 735.459$ kg \cdot m $^{-3}$), $v_e = 5$ m \cdot s $^{-1}$;
- (vi) Initial data: $h_0(y) = h_e$, $v_0(y) = v_e + (\beta_0/p_0) \int_0^y \Phi(0, z) dz$;
- (vii) Constant viscosity: $\mu_0 = 8.4 \cdot 10^{-5}$ kg \cdot m $^{-1}$ \cdot s $^{-1}$.

Initial conditions (vi) are said to be well-prepared insofar as they satisfy the divergence constraint (5a). This concept will be investigated in [1].

2.2.1. Φ linear

We first consider a linear-in-space power density: $\Phi(y) = (1 + y)\Phi_0$. This case has been evoked at the end of § 1.3.2 since it is possible to obtain explicit expressions for Θ . We thus compare on FIG. 5 numerical, exact and asymptotic enthalpies (above) as well as corresponding errors at different times (below). The error MOC/exact increases as time goes by, while the error MOC/asymptotic decreases which is expected. Indeed, the evolution of the former one is due to the addition of numerical diffusion at each time step. The latter one goes to show the convergence of the scheme. When the asymptotic state is theoretically reached (at time $t_\infty \approx 0.80$ s), the error is about 10^{-3} knowing that the mesh grid consists in only 50 nodes.

The convergence is confirmed by the results on FIG. 6. The convergence rates in norm L^∞ and in norm L^2 turn out to be of order 1. The numerical error in the scheme presented in § 2.1 is induced by the localization of the foot of the characteristic curve (of order Δt or Δt^2 depending on the formula used in ①), by the interpolation process in ② (or order Δy) and by the Euler scheme (of order Δt) in ③. Hence the global order equal to 1.

Comparisons at time 1 s are pictured on FIG. 7 for all variables involved in (5), namely h , T , ρ , v , \bar{p} and the Mach number. As each variable (except v) is computed from h , we logically observe that numerical errors are about the same. Moreover, the Mach number is about 10^{-3} all along the transient regime, which legitimates the low Mach number approach.

2.2.2. Singular charge loss

To introduce additional physical phenomena, slight modifications may be made to Syst. (5). For instance, the momentum equation (5c) can be replaced by:

$$\rho(h) [\partial_t v + v \partial_y v] - \mu_0 \partial_{yy}^2 v = -\partial_y \bar{p} - \rho(h)g - \frac{1}{2} \rho(h) v |v| \delta_{y=L/2}. \quad (5c')$$

The Dirac term is called *singular charge loss* [4, § 4.5] and models friction effects due to the presence of an element (like a mixing grid) at the middle of the core. This term only influences the pressure variable insofar as this equation is decoupled from the other ones. This is a consequence of the one-dimensional approach (the divergence constraint (5a) is sufficient to determine the velocity field in 1D but it is no longer the case in higher dimensions) and of the low Mach number framework (the density does not depend on \bar{p} through the equation of state).

Numerical results (*cf.* FIG. 8) show that the pressure decreases after the flow passed through the mixing grid.

2.2.3. Negative power density

Although this study has been carried out under the hypothesis that Φ is a positive function, theoretical results stand for negative power densities provided that $v(t, L) \geq 0$ for all time t . Otherwise, it would be necessary to have an extra boundary condition on h at $y = L$ so that the problem might be well-posed. Results are depicted on FIG. 9 for $\Phi(t, y) = -\Phi_0$. Each variable has a reversed monotonicity (except pressure) compared with the positive case.

2.2.4. Sine profile

We then take a profile that does not yield an explicit solution, namely $\Phi(y) = [1 + \sin(\frac{\bar{y}y}{L})] \Phi_0$. Φ thus vanishes at $y = 0$ and $y = L$ and is more relevant from a physical point of view as the power density seems to be

maximal at the center of the core. Results on FIG. 10 illustrate the ability of the scheme to handle non-trivial data: the asymptotic state is reached with the same order of accuracy (about 10^{-3}).

2.2.5. Alternating power density

We finally perform the simulation of the model for an unsteady (piecewise constant) power density:

$$\Phi(t) = \begin{cases} \Phi_1, & \text{if } t \in [2k\mathcal{T}, (2k+1)\mathcal{T}], k \in \mathbb{Z}, \\ \Phi_0, & \text{otherwise,} \end{cases}$$

for some $\mathcal{T} > 0$. This power density models complex situations where the heat source dramatically varies (periodically in this case), for instance when control rods fall into the core or are removed.

Theoretically speaking, the solution is expected to evolve between \bar{h}_0 and \bar{h}_1 where \bar{h}_i is the solution to Eq. (5b) for $\Phi \equiv \Phi_i$. If \mathcal{T} is large enough (*i.e.* larger than the smallest time for the system to reach the asymptotic state), the solution goes from one asymptotic state to the other.

For the computations, we set $\mathcal{T} = 1$ and $\Phi_1 = \Phi_0/5$. Results are pictured on FIG. 11: the evolution of the enthalpy is as described above.

Denoting by h_∞ the asymptotic enthalpy relatively to the constant power density $\Phi_0/5$, we see on FIG. 12 that the error $\|h_{num} - h_\infty\|_\infty / \|h_\infty\|_\infty(t)$ seems to be periodic. This shows the robustness of the scheme: the error does not increase steadily.

3. NORMAL MODE PERTURBATION

The 1D case has provided relevant qualitative results which lead to preliminary analyses. To try to obtain similar results in 2D, we are interested in a method which consists in linearizing a system of PDEs given a particular solution in order to obtain a first order approximation of solutions. In the present case, the reference state is the 1D asymptotic solution. More precisely, the inviscid 2D LMNC model reads:

$$\begin{cases} \partial_t \rho + \nabla \cdot (\rho \mathbf{u}) = 0, & (12a) \\ \partial_t (\rho h) + \nabla \cdot (\rho h \mathbf{u}) = \Phi, & (t, x, y) \in \mathbb{R}_+ \times [0, L_1] \times [0, L_2], & (12b) \\ \partial_t (\rho \mathbf{u}) + \nabla \cdot (\rho \mathbf{u} \otimes \mathbf{u} + \bar{p} \mathcal{I}_d) - \mu_0 \Delta \mathbf{u} = -\rho g \mathbf{e}_2, & (12c) \end{cases}$$

where $\mathbf{u} = (u, v)$, together with EOS (6) and initial/boundary conditions:

$$h(0, x, y) = h_0(x, y), \quad (\rho \mathbf{u})(0, x, y) = \mathbf{D}_0(x, y), \quad (13a)$$

$$h(t, x, 0) = h_e(t, x), \quad (\rho \mathbf{u})(t, x, 0) = (0, D_e(t, x)), \quad \bar{p}(t, x, L_2) = p_0, \quad (13b)$$

$$\mathbf{u} \cdot \mathbf{n}(t, 0, y) = \mathbf{u} \cdot \mathbf{n}(t, L_1, y) = 0. \quad (13c)$$

As a preliminary, we assume that $\mu_0 = 0$, $h_e(t, x) = h_e$, $D_e(t, x) = D_e$ and $\Phi(t, x, y) = \Phi(y)$. We set:

$$h^{(0)}(y) = h_e + \frac{1}{D_e} \int_0^y \Phi(z) dz, \quad \rho^{(0)}(y) = \rho(h^{(0)}(y)), \quad u^{(0)}(y) = 0, \quad v^{(0)}(y) = \frac{D_e}{\rho^{(0)}(y)},$$

and $\bar{p}^{(0)}$ such that $[\bar{p}^{(0)}]'(y) = -\rho^{(0)}(y)g - [\rho^{(0)}(y)v^{(0)}(y)^2]'$ (*cf.* Eq. (5c)). We then introduce the perturbation variables (f, r, \mathcal{P}) corresponding to the conserved variables in (12):

$$\begin{cases} \rho v h = D_e h^{(0)} + f, \\ \rho v = D_e + r, \\ \rho v^2 + \bar{p} = \frac{D_e^2}{\rho^{(0)}} + \bar{p}^{(0)} + \mathcal{P}. \end{cases} \quad (14)$$

The last variable is the first component u of the velocity field \mathbf{u} . We deduce linearizations of other variables appearing in (12):

$$\begin{aligned} h &= h^{(0)} + \frac{f - h^{(0)}r}{D_e}, & \rho &= \rho^{(0)} \left[1 - \rho^{(0)} \frac{\beta_0}{p_0} \frac{f - h^{(0)}r}{D_e} \right], \\ \rho h &= \rho^{(0)} \left[h^{(0)} + \left(1 - \frac{\beta_0}{p_0} \rho^{(0)} h^{(0)} \right) \frac{f - h^{(0)}r}{D_e} \right], & \bar{p} &= \bar{p}^{(0)} + \mathcal{P} - D_e^2 \frac{\beta_0}{p_0} \frac{f - h^{(0)}r}{D_e} - \frac{2D_e}{\rho^{(0)}} r. \end{aligned}$$

To satisfy (13c) and as the system is linear, we decompose u as $u = \sum_k e^{\sigma_k t} \sin(\xi_k x) \hat{u}_k(y)$ (Laplace transform on t and Fourier transform on x) with $\sigma_k \in \mathbb{R}$ and $\xi_k \stackrel{\text{def}}{=} \frac{2\bar{p}k}{L_1}$, $k \in \mathbb{Z}$. For the sake of simplicity, we only focus on one mode (and thus skip indices k for σ and \hat{u}). In accordance with Syst. (12), we take:

$$(f, r, \mathcal{P}) = e^{\sigma t} \cos(\xi_k x) (\hat{f}, \hat{r}, \hat{\mathcal{P}})(y).$$

Inserting these expressions in (12) leads to the linear ODE:

$$\frac{d\mathcal{U}}{dy} = \mathcal{M}(\sigma, \xi_k, y) \mathcal{U}, \quad (15)$$

with $\mathcal{U} \stackrel{\text{def}}{=} {}^t(\hat{f}, \hat{r}, \hat{\mathcal{P}}, \hat{u})$ and:

$$\mathcal{M}(\sigma, \xi_k, y) \stackrel{\text{def}}{=} \begin{pmatrix} -\sigma \frac{\rho^{(0)}}{D_e} \left(1 - \frac{\beta_0}{p_0} \rho^{(0)} h^{(0)} \right) & \sigma \frac{\rho^{(0)} h^{(0)}}{D_e} \left(1 - \frac{\beta_0}{p_0} \rho^{(0)} h^{(0)} \right) & 0 & -\xi_k \rho^{(0)} h^{(0)} \\ \sigma \frac{\beta_0}{p_0} \frac{[\rho^{(0)}]^2}{D_e} & -\sigma \frac{\beta_0}{p_0} \frac{[\rho^{(0)}]^2}{D_e} h^{(0)} & 0 & -\xi_k \rho^{(0)} \\ g \frac{\beta_0}{p_0} \frac{[\rho^{(0)}]^2}{D_e} & -g \frac{\beta_0}{p_0} \frac{[\rho^{(0)}]^2}{D_e} h^{(0)} - \sigma & 0 & -\xi_k D_e \\ -\xi_k \frac{\beta_0}{p_0} & \xi_k \left(\frac{\beta_0}{p_0} h^{(0)} - \frac{2}{\rho^{(0)}} \right) & \frac{\xi_k}{D_e} & -\sigma \frac{\rho^{(0)}}{D_e} \end{pmatrix}.$$

The characteristic polynomial of \mathcal{M} is $h_0 \left(\lambda + \frac{\sigma \rho^{(0)}}{D_e} \right)^2 (\lambda^2 - \xi_k^2)$, which means that eigenvalues are:

$$\pm \xi_k \quad \text{and} \quad \frac{-\sigma \rho^{(0)}}{D_e}.$$

The boundary conditions that supplement (15) are:

$$\hat{f}(0) = 0, \quad \hat{r}(0) = 0, \quad \hat{u}(0) = 0,$$

since conditions (13) are already satisfied by the reference state. Finally, the boundary condition on \bar{p} yields the following linear constraint:

$$\hat{\mathcal{P}}(L_2) + D_e \left(\frac{\beta_0}{p_0} h^{(0)}(L_2) - \frac{2}{\rho^{(0)}(L_2)} \right) \hat{r}(L_2) - D_e \frac{\beta_0}{p_0} \hat{f}(L_2) = 0. \quad (16)$$

We thus consider ODE (15) together with the boundary condition $\mathcal{U}(0) = {}^t(0, 0, 1, 0)$. We notice that when $\sigma = 0$ and $\xi_k = 0$ (which means that (12) reduces to (1)), we obtain $\mathcal{U}(y) = 0$ as expected. Future work will consist in solving numerically this Cauchy system and determining a relation between σ and ξ_k in order (16) to be verified.

4. CONCLUSION

We presented in this paper the first numerical simulations of the LMNC model derived in [4]. This simplified model allows to handle low Mach number fluid flows in a nuclear reactor core by means of a source term and suitable boundary conditions. The present study focuses on single-phase flow. Theoretical and numerical solutions provide relevant preliminary results.

Prospects for future works are twofold. The first one concerns the extension to the two-dimensional case. We plan to carry on exploring the perturbation approach to provide approximated solutions in 2D and paying attention to the regularity of solutions: expressions derived in the paper turn out to be 1D strong solutions to the LMNC model as soon as $\Phi \in \mathcal{C}^2(0, L)$. Nevertheless, the concept of weak solutions will have to be designed when Φ is less regular. We also contemplate obtaining similar 2D explicit solutions by means of the method of characteristics even if the success of this method applied to the LMNC model relies heavily on the one-dimensional property.

As for the numerical part, an extension of the MOC scheme to 2D will be considered especially for cartesian grids. Dealing with unstructured grids requires an efficient localization procedure. Another strategy will be to design a finite-volume method applied to a conservative formulation of the model. An idea will be to adapt the code from [3] to our problem. The latter code solves the incompressible Navier-Stokes equations. Source terms must be implemented in order to take the (non-free) divergence constraint and the power density into account.

The second prospect will be the enrichment of the model. Indeed, several physical phenomena have to be modelled like phase transition. This will be processed in [1] since some steam may appear at the top of the core. We will also have to focus on the equation of state insofar as the stiffened gas law may be limited in the present range of temperatures. More evolved equations of state (Van der Waals or Peng-Robinson EOS) as well as tabulated laws will be considered. Other phenomena may be taken into account such as thermal diffusion or coupling with radioactive decay phenomena. Simulations might show whether these phenomena can be neglected. The modelling of the power density will also be enhanced with additional dependence with respect to thermodynamic variables.

Acknowledgments. This CEMRACS project was funded by INRIA (EPI SIMPAF) and CEA (DEN/DANS/DM2S). The authors also thank the organizers of the 2011 session.

REFERENCES

- [1] M. BERNARD, S. DELLACHERIE, G. FACCANONI, B. GREC and Y. PENEL. *Study of a low Mach nuclear core model for two-phase flows with phase transition I: stiffened gas law.* (in preparation).
- [2] S. DELLACHERIE, G. FACCANONI, B. GREC and Y. PENEL. *Study of a low Mach nuclear core model for two-phase flows with phase transition II: tabulated EOS.* (in preparation).
- [3] C. CALGARO, E. CREUSÉ and T. GOUDON. *A hybrid finite volume – finite element method for variable density incompressible flows.* **J. Comput. Phys.**, 227(9), 4671–4696 (2008).
- [4] S. DELLACHERIE. *On a low Mach nuclear core model.* **ESAIM: Proceedings**, (to appear).
- [5] S. DELLACHERIE. *On a diphasic low Mach number system.* **Math. Model. and Num. Anal.**, 39(3), 487–514 (2005).
- [6] D. DURRAN. *Numerical Methods for Fluid Dynamics: with Application to Geophysics.* **Springer**, Texts in Applied Mathematics 32, (2010).
- [7] O. LE MÉTAYER, J. MASSONI and R. SAUREL. *Elaborating equations of state of a liquid and its vapor for two-phase flow models.* **Int. J. Therm. Sci.**, 43(3), 265–276 (2004).
- [8] O. LE MÉTAYER, J. MASSONI and R. SAUREL. *Modelling evaporation fronts with reactive Riemann solvers.* **J. Comput. Phys.**, 205(2), 567–610 (2005).
- [9] E. W. LEMMON, M. O. MCLINDEN and D. G. FRIEND. *Thermophysical properties of fluid systems.* In WebBook de Chimie NIST, Base de Données Standard de Référence NIST Numéro 69, Eds. P.J. LINSTROM and W.G. MALLARD, National Institute of Standards and Technology, Gaithersburg MD, 20899,
- [10] A. MAJDA & J. SETHIAN. *The derivation and numerical solution of the equations for zero mach number combustion.* **Combust. Sci. Technol.**, 42, 185–205 (1985).
- [11] Y. PENEL. *An explicit stable numerical scheme for the 1D transport equation.* **DCDS-S**, 5(3), 641–656 (2012).

- [12] Y. PENEL. *Étude théorique et numérique de la déformation d'une interface séparant deux fluides non-miscibles à bas nombre de Mach*. PhD Thesis, Université Paris 13, France (December 2010).
- [13] N. TODREAS & M. KAZIMI. *Nuclear Systems I: Thermal Hydraulic Fundamentals*. **Taylor & Francis Group**, 2nd edition, (2011).

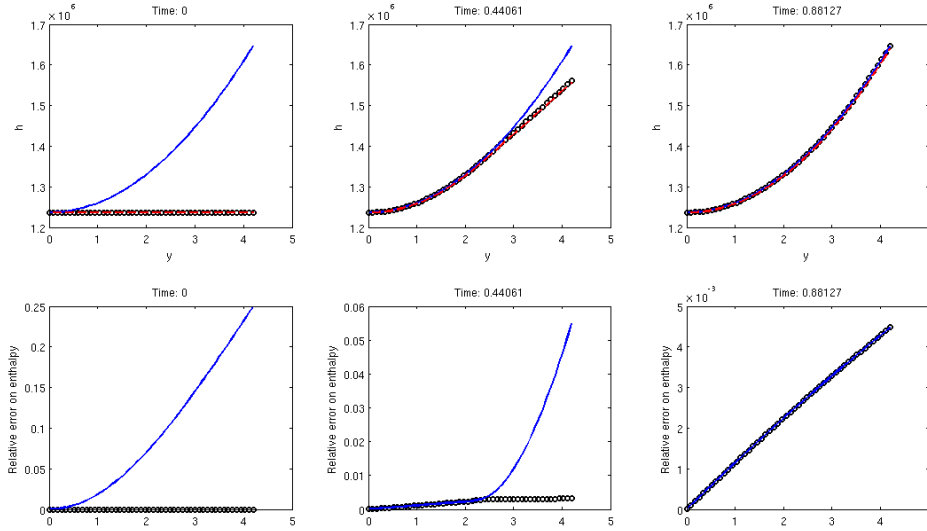


FIGURE 5. **Linear case.** *Above:* numerical (red dashed line), exact (black circles) and asymptotic (blue solid line) solutions to Eq. (5b) at different times. *Below:* relative error between numerical and exact solutions (black circles) and between numerical and asymptotic solutions (blue solid line) at different times.

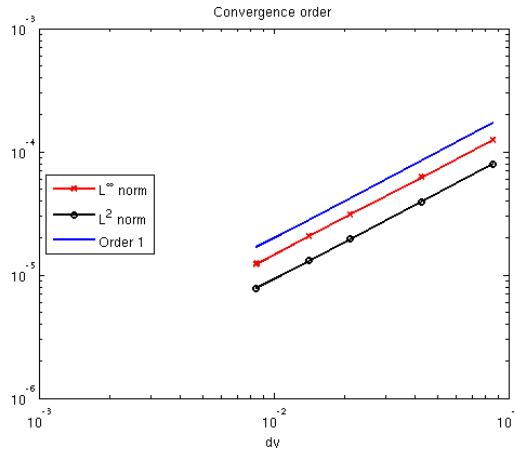


FIGURE 6. **Linear case.** Convergence rate (logarithmic scale) in norms L^∞ and L^2 .

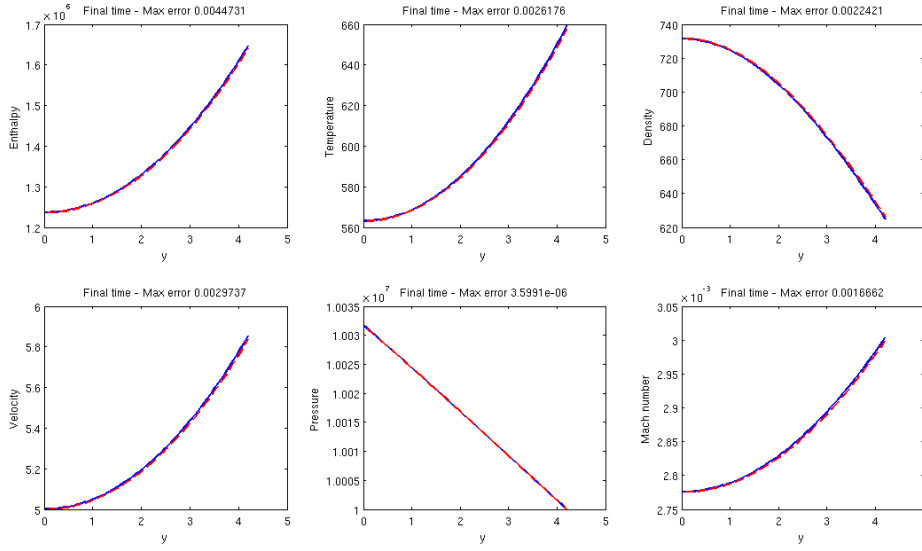


FIGURE 7. **Linear case.** Comparison at time $t = 1$ s between numerical (red dashed line) and asymptotic solutions (blue solid line) to Syst. (5).

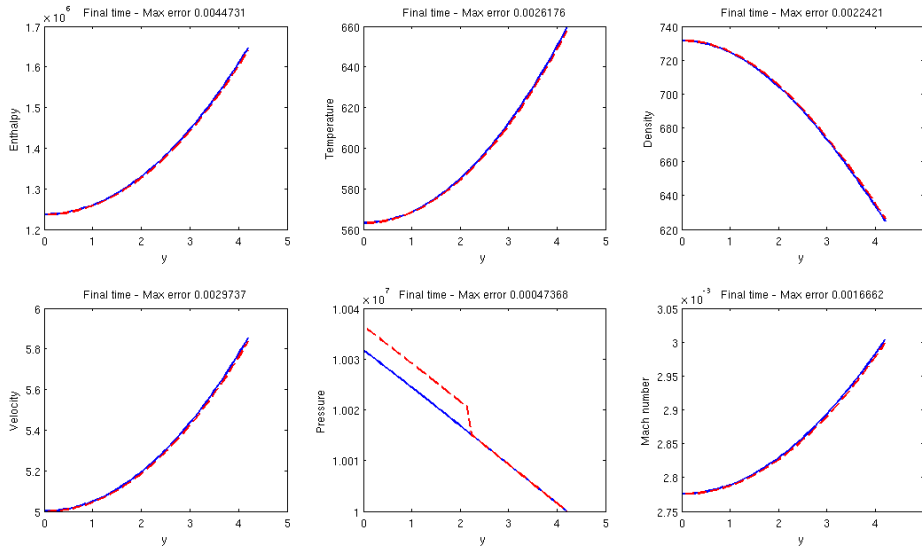


FIGURE 8. **Linear case (with singular charge loss).** Comparison at time $t = 1$ s between numerical (red dashed line) solutions to Syst. (5) with (5c) replaced by (5c') and asymptotic solutions (blue solid line) to Syst. (5).

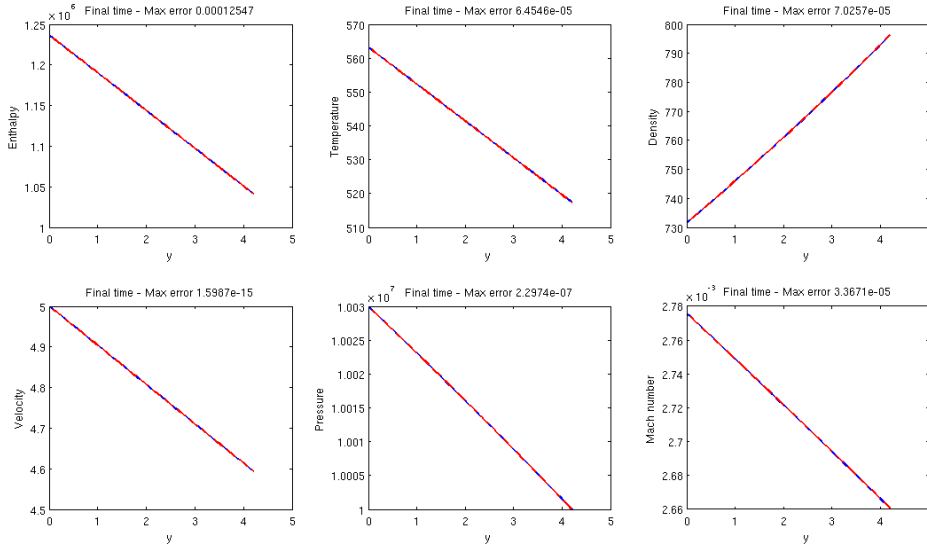


FIGURE 9. **Negative Φ case.** Comparison at time $t = 1$ s between numerical (red dashed line) and asymptotic solutions (blue solid line) to Syst. (5).

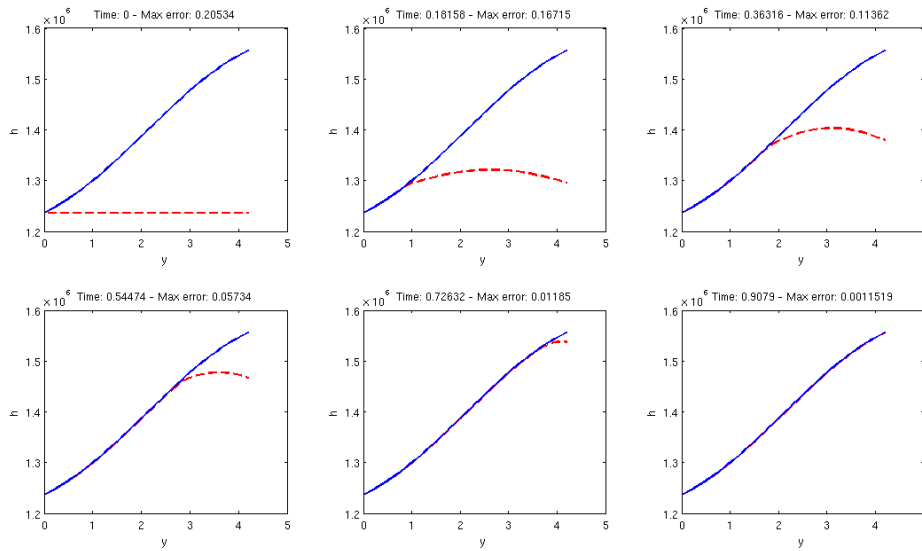


FIGURE 10. **Sine case.** Numerical (red dashed line) and asymptotic (blue solid line) solutions to Eq. (5b) at different times.

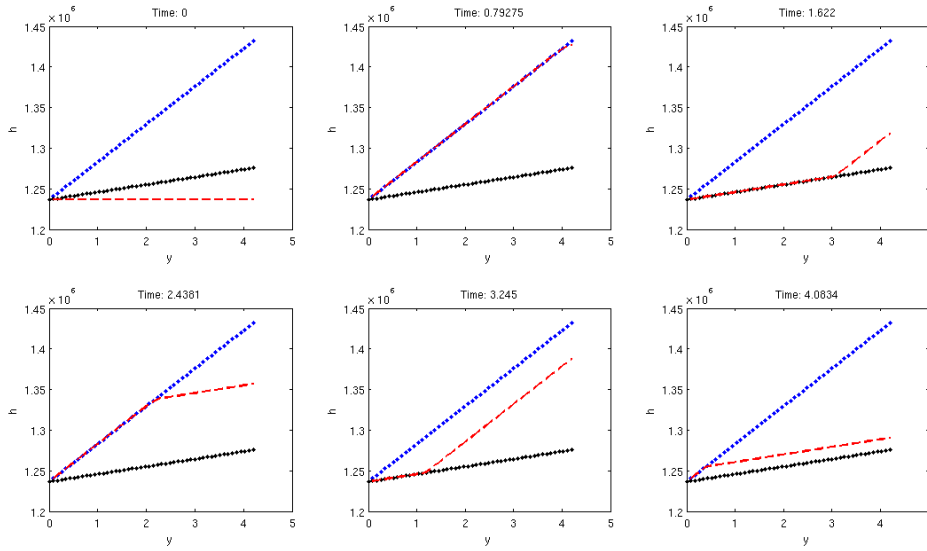


FIGURE 11. **Alternating Φ case.** Numerical (red dashed line) and asymptotic (associated to Φ_0 – blue dotted line and to $\Phi_0/5$ – black dotted line) solutions to Eq. (5b) at different times.

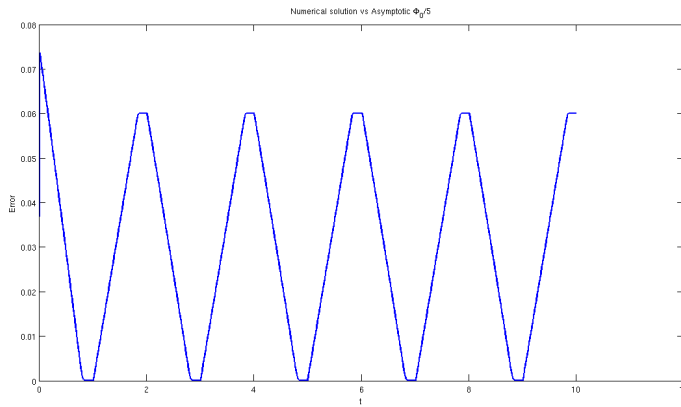


FIGURE 12. **Alternating Φ case.** Evolution with respect to time of the error between numerical solution to Eq. (5b) and asymptotic solution associated to $\Phi_0/5$.